International Journal of Impact Engineering 46 (2012) 1–10

Contents lists available at SciVerse ScienceDirect

International Journal of Impact Engineering

journal homepage: www.elsevier.com/locate/ijimpeng

The compressive response of porcine adipose tissue from low to high strain rate

Kerstyn Comley, Norman Fleck*

Cambridge University Engineering Department, Trumpington Street, Cambridge CB1 2PZ, UK

ARTICLE INFO

Article history:
Received 2 May 2011
Received in revised form
31 October 2011
Accepted 20 December 2011
Available online 1 February 2012

Keywords:
Adipose tissue
Split Hopkinson pressure bar
Constitutive testing
Ogden model

ABSTRACT

Subcutaneous adipose tissue has been tested in uniaxial compression over a wide range of strain rates from quasi-static to 5700 s^{-1}. In the quasi-static regime, the tissue was subjected to fully reversed cyclic loading. A symmetric tensile-compressive response was observed with lock-up at tensile and compressive strains of 25%. Uniaxial compressive tests at high strain rates (1000 s^{-1}–5700 s^{-1}) were conducted with a split Hopkinson pressure bar (SHPB) using polycarbonate bars. Over the full range of strain rate from quasi-static to high strain rate, the magnitude of stress increases with strain rate whereas the shape of the stress versus strain response is invariant: the stress level scales with the initial modulus *E*. A one term Ogden energy density function is adequate for describing the shape of the stress versus strain response at any given strain rate.

1. Introduction

Subcutaneous adipose tissue is a soft connective tissue located directly beneath the dermis. The tissue fulfils a wide variety of multifunctional roles: it provides thermal insulation, allows for energy storage, and acts as a shock mitigator, yet it must possess a sufficiently low stiffness in order to allow for the free movement of underlying muscle groups. In order to obtain accurate engineering models for tissue damage due to dynamic loading, such as air blast and sand blast, sports injury and high rate needle-free drug delivery, there is a need to measure the high strain rate response of adipose tissue and to use these data to suggest appropriate constitutive descriptions. Recently, Shergold and Fleck [1] have developed a theoretical model for deep penetration of the dermis. In order to apply this model to adipose tissue it is necessary to measure the uniaxial response over a wide range of strain and strain rate.

The purpose of the present study is to examine the uniaxial response of adipose tissue at strain rates over the range 10^{-4} s^{-1}–5000 s^{-1}. Both monotonic and cyclic tests are performed. The quasi-static tests entail large amplitude, fully reversed loading in order to probe the non-linear uniaxial response and to determine the degree of asymmetry between the tensile and compressive responses. Measurements of the uniaxial compressive tests at high strain rates (1000 s^{-1}–5700 s^{-1}) are made using a split Hopkinson pressure bar (SHPB) with polycarbonate bars (PC). It is demonstrated that a one dimensional Ogden model provides an adequate fit to the data over the full range of strain rates employed. We begin with a summary of the microstructure of adipose tissue, and then review test methods that have been developed for measurement of the uniaxial response of soft tissue.

1.1. Microstructure of adipose tissue

Adipose tissue, commonly known as fat, is a connective tissue comprising lipid-filled cells called adipocytes, as sketched in Fig. 1. The lipid is a triacylglyceride whose molecular weight is on the order of 900 g mol^{-1}. Comley and Fleck [2] have recently found that the viscosity of the lipid is $\eta = 36.8$ mPa s at 37 °C; this is sufficiently small for the lipid to give negligible contribution to the macroscopic response of the adipose tissue. Comley and Fleck [2] also measured the viscoelastic response of the lipid: the storage shear modulus is on the order of $G_l = 0.01$ Pa which is much less than that of adipose tissue. Consequently, the lipid can be treated as an incompressible inviscid fluid that enforces material incompressibility. 60–80% by weight of adipose tissue is lipid, 5–30% is water and the remaining 2–3% is protein [3]. Histology of adipose tissue suggests that it is approximately isotropic in structure and is thereby isotropic in mechanical properties [4].

Each adipocyte comprises a single lipid vacuole and a nucleus within a phospholipid bilayer. The adipocytes are of diameter 80 μm and are supported by two collagen-based structures, as detailed by Comley and Fleck [2]:

(i) *Reinforced basement membrane* – a collagen mesh, containing type I and IV collagen, surrounding each cell. The reinforced

* Corresponding author. Tel.: +44 1223 748240.
E-mail address: naf1@eng.cam.ac.uk (N. Fleck).

0734-743X/$ – see front matter © 2012 Elsevier Ltd. All rights reserved.
doi:10.1016/j.ijimpeng.2011.12.009

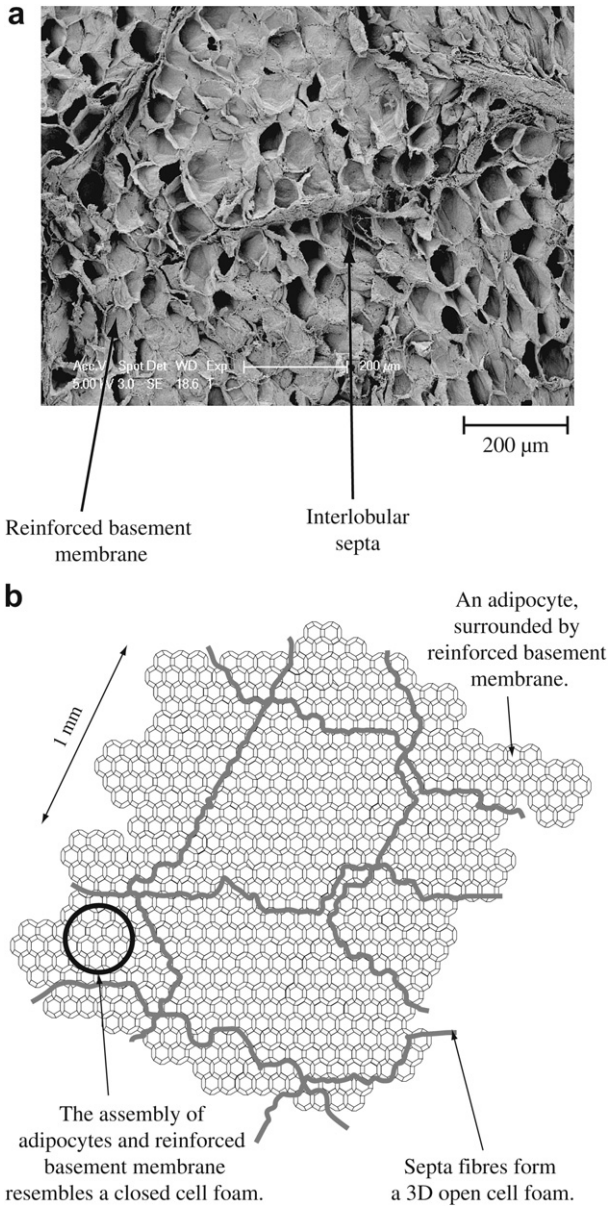

Fig. 1. (a) Scanning electron microscope (SEM) image, showing the reinforced basement membrane that surrounds each adipocyte and an interpenetrating septa fibre, (b) A sketch of a lobule of adipose tissue.

basement membrane behaves as a closed cell foam, and dictates the macroscopic stress-strain behaviour and macroscopic toughness.

(ii) *Interlobular septa* – a type I collagen fibre network which, takes the form of an open cell 3D foam. The septa bundles are several millimetres in length and can range in diameter from 10 nm (for a single fibre) to 30 μm (for a bundle of fibres). They share a similar structure to that of fibrous collagen bundles in the dermis. In contrast to the dermis, the volume fraction of interlobular septa in adipose tissue is sufficiently low that it provides a negligible contribution to the macroscopic modulus.

The intervening space in adipose tissue is filled with *ground substance*. The ground substance (which fills the open channels) accounts for only a few percent of the volume fraction in adipose tissue and there is negligible free fluid available to endow the tissue with poro-elastic properties [5,6]. This has been confirmed by preliminary compression tests on porcine adipose tissue. On subjecting the tissue to a uniaxial compressive strain of 50% the volume of liquid expressed was less than 1% of the overall volume. Therefore, throughout this investigation, adipose tissue is treated as a non-porous viscoelastic solid.

Comley and Fleck [2] made use of microstructural observations and macroscopic measurements of modulus in order to develop a micromechanical model for the stiffness of porcine adipose tissue. The models suggest that adipose tissue behaves as a closed cell foam such that the effective modulus is controlled by the stiffness of the reinforced basement membrane. The effect of volumetric constraint by the liquid is to increase slightly the effective stiffness of the reinforced basement membrane. The septa fibres play only a secondary role in dictating the macroscopic modulus.

1.2. Review of methods used to measure the constitutive response of soft tissue

The measurement of the constitutive properties of biological tissues tends to focus on either the compressive or tensile properties of the tissue. For example, Miller-Young et al. [7] measured the stress versus strain response of calcaneal fat in unconfined uniaxial compression at strain rates up to 35 s^{-1}. Samani et al. [4] used an indentation method to measure the compressive modulus of breast tissue while Zheng and Mak [8] have attempted to determine the properties of soft limb tissue by manual indentation of live subjects. Although there are no data reported in the literature for the tensile properties of adipose tissue, uniaxial tensile data exist for other soft biological tissues. For example, Huang et al. [9] performed tensile tests and compression tests on cartilage. When testing soft tissues there is practical difficulty in identifying the zero strain datum: the Young's modulus is low and consequently a pre-stretch or pre-tension can be generated within the tissue during insertion into a test machine. This raises the question as to whether the transition point between tension and compression has been accurately identified. Sophisticated methods which attempt to overcome these difficulties have been presented, see for example Mansour et al. [10]. However, these methods do not guarantee that the relaxed reference state of zero strain has been identified. This problem is resolved in the current study by performing large amplitude fully reversed strain excursions.

The split Hopkinson pressure bar (SHPB) is an established technique used to measure the behaviour of many engineering materials at strain rates above 100 s^{-1}. In order to increase the measurement sensitivity, modifications are needed to the standard set-up based on a steel bar. Song et al. [11] measured the properties of porcine muscle with aluminium pressure bars, and Shergold et al. [12] used magnesium bars to measure the stress versus strain response of pig skin. In this study a modified SHPB makes use of polycarbonate (PC) bars. Polymeric pressure bars are attractive because they have a low Young's modulus on the order of 3 GPa and thereby give a more sensitive response than metallic bars.

The interpretation of Hopkinson bar tests on soft solids is made complicated by the effects of material inertia within the specimen, as follows. Axial and radial inertia lead to a non-uniform stress state along the axis of the specimen [13,14], and must be taken into account in data reduction. In SHPB tests on porcine muscle, Song et al. [11] observed an axial stress of 2 MPa at low compressive strains due to radial inertia, prompting them to change the specimen geometry from solid cylindrical to an annulus. This method was attempted in preliminary tests in the present study but found to be impractical for the case of adipose tissue: it was difficult to prepare annular specimens with stable dimensions.

Currently, there is no consensus within the literature on the preferred method for data reduction in PC Hopkinson bar tests. The

open issue is whether the degree of viscoelasticity of the PC is sufficiently high to require a viscoelastic analysis or whether a simpler, elastic analysis suffices. Wang et al. [15] assessed the viscoelastic properties of PMMA and PC for Hopkinson bar application, and concluded that the degree of longitudinal wave attenuation along the bar is minor for PC but significant for PMMA. Also, they analysed the degree of wave dispersion expected for PMMA and PC; their analysis suggests minor effects for PC but significant dispersion effects within PMMA. Subsequently, other investigators have used PMMA bars and employed a viscoelastic analysis in data reduction [16,17]. This has led to the expectation that a viscoelastic analysis is necessary for all polymeric bars. However, Deshpande and Fleck [18] have demonstrated that an elastic analysis suffices for PC bars in their Hopkinson bar tests on metallic foams. The validity of using the SHPB with PC bars to test adipose tissue is demonstrated in Appendix A.

2. Experimental methods

Compression tests were performed over 3 strain rate regimes:

1. High strain rate tests (1000 s^{-1}–5700 s^{-1}), using the split Hopkinson pressure bar.
2. Intermediate strain rate tests (20 s^{-1}–260 s^{-1}), using a servo-hydraulic test machine; and
3. Low strain rate tests (2×10^{-3} s^{-1}–0.2 s^{-1}), using a screw-driven test machine. Additionally, a limited number of fully reversed tests were performed at low strain rate by adhering the end faces of the specimen to the loading platens of the screw-driven test machine.

All tests were conducted at room temperature in ambient air at 25 °C and 50% relative humidity. During testing, specimens were kept hydrated with a saline spray. A circular cylindrical geometry was employed, as follows.

2.1. Specimen preparation for all tests

It is difficult to acquire fresh human subcutaneous adipose tissue for ethical, immunological and practical reasons. Since porcine adipose tissue has similar morphology, histology and cell kinetics to human adipose [19], it has been chosen as a suitable substitute. Samples of dermis and subcutaneous fat were removed from the jowl of the pigs to a depth of 20 mm immediately after slaughter. The samples were stored in phosphate buffered saline (PBS) at room temperature, and testing always commenced within 3 h of slaughter.

Specimens were prepared following the method described by Miller-Young et al. [7], but without partial freezing. Circular cylindrical specimens of adipose tissue were cut to a diameter $d = 10$ mm using sharp metal punches, such that the axis of the specimen was aligned with the unit normal to the outer surface of the skin. These samples were then end-trimmed by a cutting tool so that their ends were flat and parallel. The cutting tool comprised two parallel razor blades bonded to the ends of a PMMA block, with fresh razor blades used for each test. The block length defined the nominal specimen length (3 mm for high and medium strain rates and 8 mm for low strain rates). Before testing the length and diameter of each specimen in the unstressed state was measured using callipers.

The SHPB tests were performed on specimens of reduced gauge length in order to minimise wave propagation effects along the axis of the specimen, as discussed by Song et al. [11] and Shergold et al. [12]. Low strain rate tests were performed on specimens of gauge length in the range 3 mm–8 mm and there was no significant difference in response, thereby justifying the high strain rate data at a gauge length of 3 mm.

2.2. High strain rate tests

The high strain rate compression tests were conducted using an SHPB with PC bars of diameter 12 mm. The input and output bars were of length $L_b = 1.1$ m and the striker bar was of length 0.25 m. Electrical resistance strain gauges were bonded at mid-length of the input and output bars, see Fig. 2. The gauges were placed as diametrically opposed pairs, in order to check for bending, and were calibrated using a shunt resistor following Dally and Reily [20]. The theory of elastic wave propagation in longitudinal bars was used to convert the strain gauge data into the nominal stress versus nominal strain response of the adipose tissue [21].

For each test the relaxed length of specimen was first measured, and the gap between Hopkinson bars was adjusted to this measured value. This ensures that the high strain rate tests had the correct zero strain datum.

2.3. Intermediate strain rate tests

Specimens were compressed at a prescribed displacement rate between smooth nylon platens, using a servo-hydraulic tensile test machine and a purpose built load cell [22]. The load cell comprised an aluminium beam, fitted with four strain gauges in a Wheatsone bridge arrangement. The stiffness and sensitivity of the beam were 20.46 N mm^{-1} and 141 $\mu\varepsilon$ N^{-1}, respectively [23]. The displacement of the machine platens was measured using a linear resistance displacement transducer (LRDT) mounted as an integral part of the test machine. Care was taken to subtract off the machine (and load cell) compliance from the measured displacement response. The outputs from the beam transducer and LRDT were converted to nominal engineering stress, strain and strain rate.

Initially, in each test, there was a gap of 2 mm between specimen and the platens. This ensured that the moving platen had attained the desired test velocity prior to contact with the specimen. The deceleration phase of the moving platen began when the specimen thickness had been reduced to 3 mm (from an initial height of 8 mm) and arrest occurred when the specimen was of thickness 1 mm. Thus, the platen was moving at a constant velocity for compressive nominal strains of up to 60%, which encompasses the regime of interest in the study.

2.4. Low strain rate tests

Cylindrical specimens were compressed between smooth 15 mm thick nylon platens at a prescribed velocity $\dot{u}$ using a screw-driven tensile test machine. The loads were recorded via a 5 N load cell capable of measuring 20 mN to within 1%. The determination of the point of zero strain is difficult to define as the stress levels in the region of zero strain are comparable to the resolution of the test machine. We adopt the procedure of Miller-Young et al. [7] and define the zero strain point (and hence the initial length) to correspond to the point at which a force is first detectable on the load cell (on the order of 10 mN). A limited number of low strain rate tests were also carried out to more closely mimic *in-vivo* conditions: the tissue was fully saturated in saline at 37 °C for 1 h prior to testing and

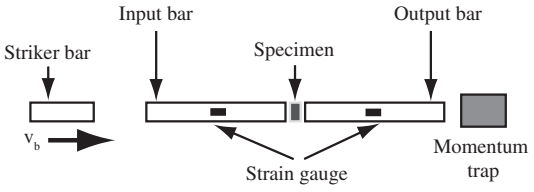

Fig. 2. Set-up of the split Hopkinson pressure bar.

this was maintained during each test. Fully reversed loading experiments were also conducted using the same set-up as that described above for compression testing at low strain. The upper and lower faces of the specimens were bonded to the platens using a cyanoacrylate adhesive (Loctite® Super Glue™ Control Liquid). A displacement-time waveform of periodic triangular shape was used to enforce alternating strain at a strain rate of 0.07 s^{-1}. Prior to cyclic testing, a preliminary compression test was conducted to examine whether the constraint associated with bonding of the tissue to the platens resulted in an increase in axial stress. No significant difference in response was observed for the bonded and unbonded specimens, and this justified the gripping arrangement in the cyclic tests.

2.5. Lubrication of specimens during testing

The specimens were self-lubricated by a small degree of seepage of triglyceride from the cut ends and no additional lubrication was needed. To validate this, 20 additional tests were performed at low strain rate with (i) additional lubrication using petroleum jelly (as commonly used in Hopkinson bar testing [24]) or (ii) cyanoacrylate adhesive applied to the ends of the specimen in order to give full bonding to the platens. These changes in boundary condition did not affect the measured responses to within experimental scatter (not shown for the sake of brevity). This justifies the use of self-lubricated specimens.

3. Results

First, consider the high strain rate Hopkinson bar tests. A representative oscilloscope trace of the strain history in the pressure bars at a strain rate of 1840 s^{-1} is shown in Fig. 3. The reflected trace in Fig. 3 is of the same length as the input pulse. However, the test is complete at a time of 1 ms as this corresponds to a very high compressive strain in the sample (on the order of 0.4). Consequently, the reflected pulse is not shown beyond 1 ms. The strain history in the input bar is the characteristic square pulse expected for a linear, elastic impact event between striker and input bar. It is clear from the large value of strain (on the order of 1 mε) detected in the output bar that PC is a suitable choice in terms of sensitivity. It is demonstrated in Appendix B that the material inertia of the test specimen contributes significantly to the measured axial stress over the first 8% of axial strain. An assessment of this inertial stress contribution is made in Appendix B and this contribution is subtracted from the observed stress versus strain response. The net stress versus strain response is shown in Fig. 4 for each of the high strain rate tests. The degree of material scatter is sufficiently high to mask any sensitivity of response to strain rate over the relatively narrow range of 1000 s^{-1}–5700 s^{-1} employed in the Hopkinson bar tests. The authors believe that the scatter is real, and is intrinsic to the adipose tissue. This degree of scatter is comparable to that observed in other soft tissue, see for example [25]. However, the sensitivity to strain rate becomes clear once the response at low and intermediate strain rate are taken into consideration, as follows.

The compressive response at low strain rates (2×10^{-3} s^{-1}–2 s^{-1}) and at intermediate strain rates (20 s^{-1}–260 s^{-1}) are given in Figs. 5 and 6, respectively. There is comparable scatter within each test regime, but a significant difference in stress level exists for the low, intermediate and high strain rate regimes, compare Figs. 4–6. This is further illustrated in Fig. 7, wherein the logarithm of nominal stress is plotted against nominal strain. The results for low strain rate tests in saline at 37 °C are included (as dotted lines) in Fig. 5; we conclude that there is no significant difference in response between the simulated *in-vivo* conditions and the ambient tests in air at room temperature. This is consistent with previous observation that the contribution to the macroscopic stress-strain response from the temperature-sensitive lipid is negligible [2].

The measured quasi-static cyclic response of adipose tissue under fully reversed loading at 0.06 Hz is reported in Fig. 8a. The results are presented as the averaged stress over four cycles for a representative specimen. The levels of force measured in the central linear portion of the curve are of the order of 50 mN, making it difficult to identify the point of zero strain. Therefore, the zero strain datum was taken as mid-way between the points of strain at which the stress equals ±1 kPa. The data takes the form of a hysteresis loop with the central portion of the curve spanning a strain range of 50%. This portion is approximately linear with a tangent modulus of 1 kPa. At strains greater than approximately ± 25% strain, the tissue 'locks-up'. The shapes of the tensile and compressive portions are compared in Fig. 8b and are almost symmetrical and confirms our procedure for identifying the point of zero strain. This contrasts with the pronounced asymmetry of other biological tissues such as cartilage and bone [26,27].

3.1. Role of material scatter

Preliminary tests were performed on the same area of a pig, and on different pigs in order to assess the degree of variability in the data. For example, at a loading rate of 0.002 s^{-1}, twenty tests were

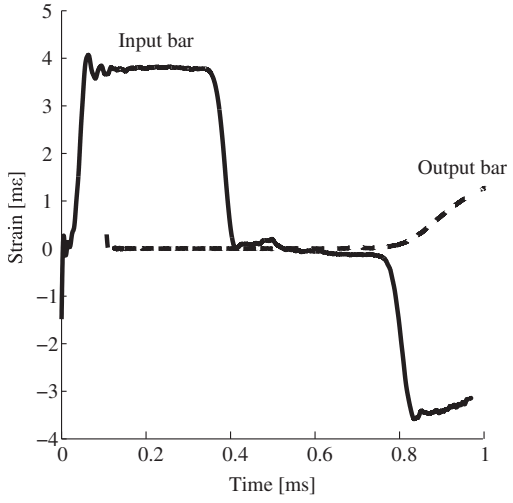

Fig. 3. Oscilloscope trace of the compression of adipose tissue using a split Hopkinson pressure bar at a strain rate of 1840 s^{-1}.

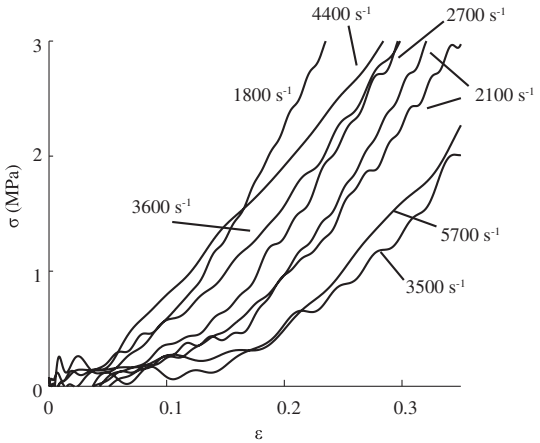

Fig. 4. Unconfined uniaxial compression of adipose tissue using split Hopkinson pressure bar at strain rates of 1000–5700 s^{-1}.

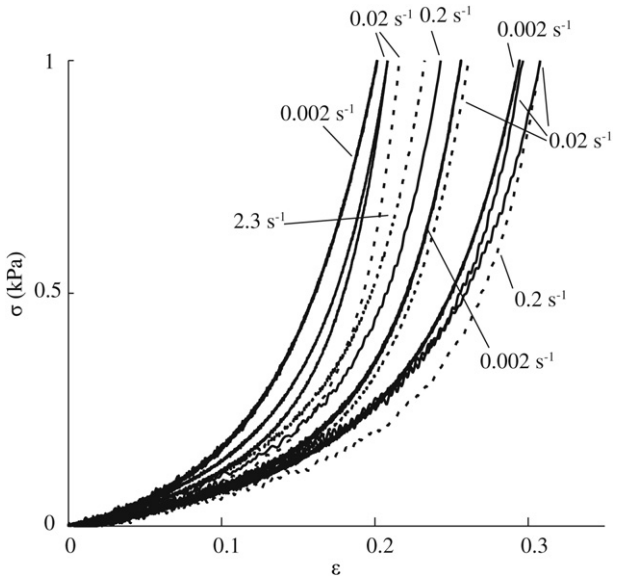

Fig. 5. Uniaxial compression of adipose tissue at strain rates in the range 0.002–0.25 s^{-1}. A solid line denotes data at 25 °C and a dotted line denotes data for tests in saline at 37 °C.

performed on specimens from the same pig. Likewise, 5 tests were performed on five different pigs. The degree of scatter can be quantified as follows. The level of uniaxial compressive stress at a strain of 0.1 was recorded for the twenty tests on the same pig, and gave a mean value of 115 Pa, and a standard deviation of 20 Pa. For the five tests on five pigs, the mean stress was 85 Pa and the standard deviation was 25 Pa. We conclude that the test variability from different parts of the same pig is comparable to that from pig to pig. Although the scatter is high, the main purpose of the present study is to obtain order-of-magnitude measures of the compressive response of porcine tissue over a wide range of strain rate. The increase in stress level when the strain rate is increased from quasi-static rates to those characteristic of a split Hopkinson bar far exceeds the degree of material scatter, recall Fig. 7.

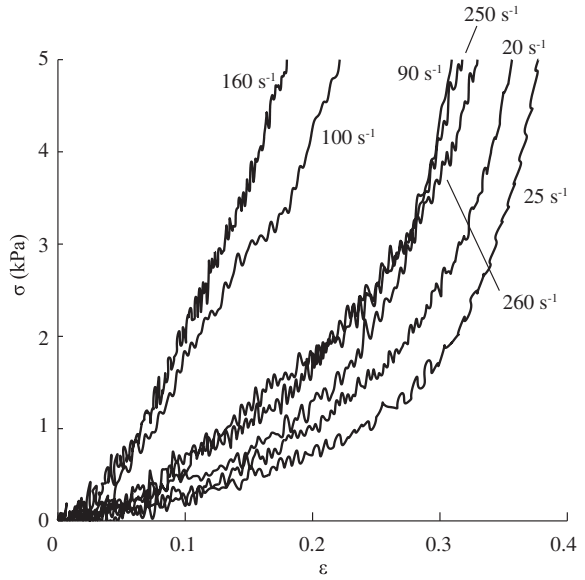

Fig. 6. Unconfined uniaxial compression of adipose tissue at strain rates in the range 20–260 s^{-1}.

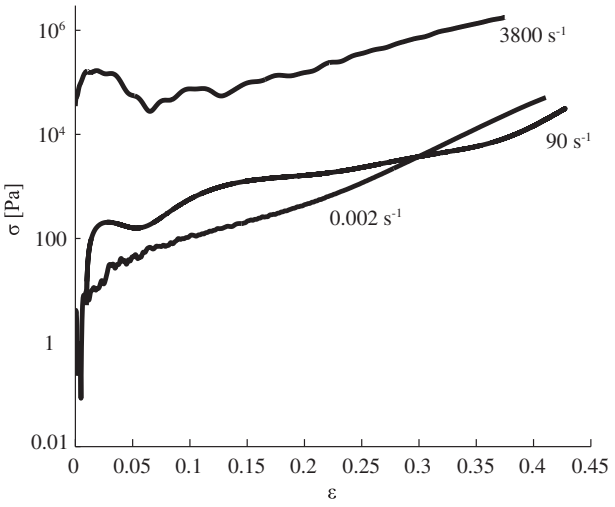

Fig. 7. Selected results for uniaxial compression over the span of strain rates.

4. Interpretation of results

It is instructive to explore the sensitivity of Young's modulus and stress-strain curve to strain rate. At high strain rate, the requirement of subtracting off an inertial contribution to stress over the first 8% of strain leads to inaccurate values of Young's modulus; consequently, a secant modulus at a strain level of 10% is used to explore the variation in Young's modulus with strain rate. The dependence of E upon $\dot{\varepsilon}$ is plotted in Fig. 9a. For strain rates in the range 2×10^{-3} s^{-2}–10 s^{-1} E equals approximately 1 kPa and is insensitive to strain rate. In contrast, the Young's modulus increases by three orders of magnitude from $E = 2$ kPa at $\dot{\varepsilon} = 10$ s^{-1} to approximately $E = 4$ MPa at $\dot{\varepsilon} = 3000$ s^{-1}.

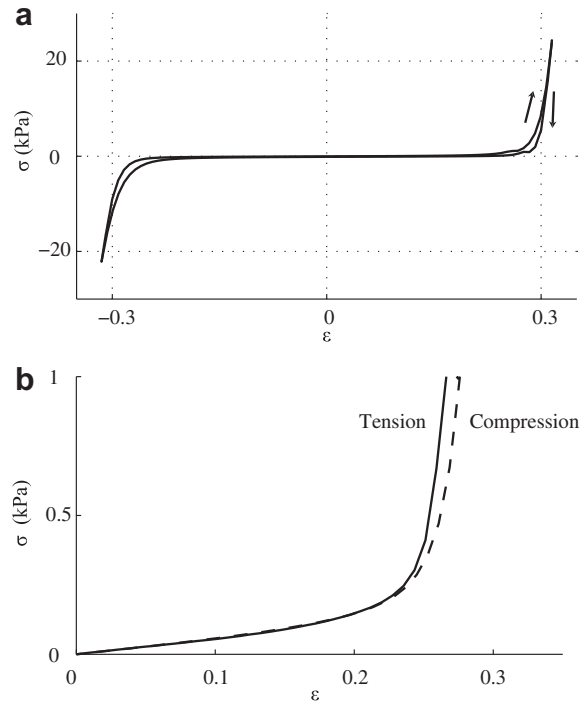

Fig. 8. (a) Quasi-static uniaxial compression and tension of adipose tissue averaged over 4 cycles. Arrows show the direction of displacement. The data has been shifted relative to the strain axis so that strain is equi-distant between ±1 kPa stress. (b) Quasi-static uniaxial tension versus compression of adipose tissue.

The measured value of E at low strain rate agrees with previous measurements for adipose tissue to within an order of magnitude, as follows [4,7,28–30]. Miller-Young et al. [7] measured a uniaxial compression modulus of 5 kPa for human calcaneal fat; Samani et al. [4] used indentation to measure an elastic modulus of 1.9 kPa for breast tissue; and Nightingale et al. [30] measured a value of 5 kPa for human abdominal subcutaneous tissue using acoustic radiation force impulse imaging (ARFT).

It is clear from Fig. 9a that a switch in strain rate sensitivity occurs at a strain rate of about 10 s^{-1}. This is consistent with the observations on adipose tissue by Gefen and Haberman [31] over a strain rate regime of 6–44 s^{-1}, and by Miller-Young et al. [7] over a strain rate regime of 10^{-3} to 35 s^{-1}. A similar sensitivity has been observed for muscle by Van Sligtenhorst et al. [32] and Song et al. [11] for strain rates in the range 10^{-3} s^{-1}–3700 s^{-1}. The dependence of E upon $\dot{\varepsilon}$ for porcine dermis is included in Fig. 9a (and Table 1), as taken from Shergold et al. [12]. We conclude that the dermis is stiffer than adipose tissue by more than two orders of magnitude at low strain rates but has a comparable modulus at high strain rate.

Shergold et al. [12] have shown that the shape of the stress-strain curve is invariant to changes in strain rate, resulting in a unique plot of σ/E versus, see Fig. 9b. To explore whether the shape of the stress-strain curve of adipose tissue is similarly invariant to strain rate, we have added to Fig. 9b the plots of σ/E versus ε from the present study. In broad terms, the data collapse onto a single master curve to within material scatter. Further, the normalised response for adipose tissue and the dermis are similar at low strain levels (below 0.2); we note, however, that adipose tissue has a lower lock-up strain of 0.25 compared to the value of 0.4 for the dermis.

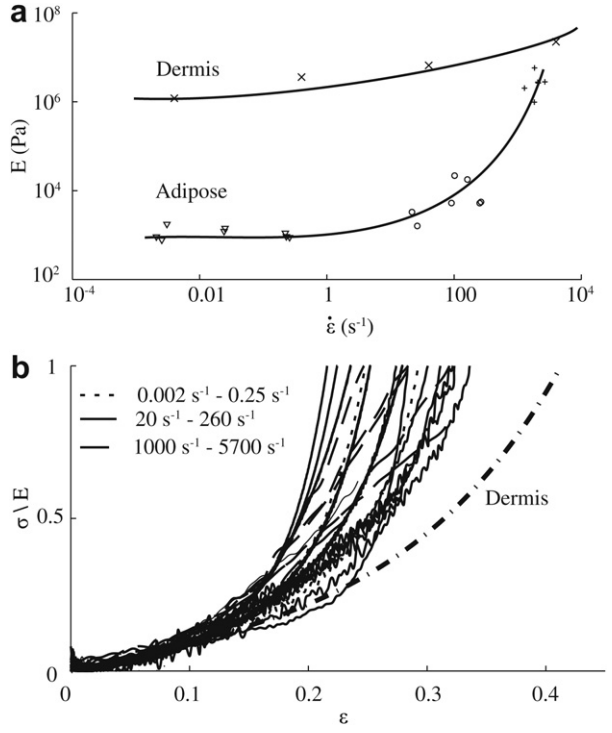

Fig. 9. (a) Modulus, E of adipose tissue under uniaxial compression versus strain rate $\dot{\varepsilon}$. Data shown by triangular markers were measured using a screw-driven tensile test machine, circular markers by a hydraulic test machine and the crosses represent data collected using the SHPB. Diagonal crosses represent the modulus of dermis recorded by Shergold et al. [12]. (b) Stress versus strain curves of adipose tissue, normalised by modulus E. The average dermal response measured by Shergold et al. [12] is shown for comparison.

Table 1
Best fit values (for μ) for a one term Ogden strain energy density function of adipose and dermal tissue evaluated at different strain rates, $\dot{\varepsilon}$. Values for the dermis are taken from Shergold et al. [12].

$\dot{\varepsilon}$ (s^{-1})	Adipose μ (kPa)	Dermis μ (kPa)
0–10	0.4	400
20–260	1.7	2200
1000–5700	1120	7500

5. Curve fitting of the Ogden constitutive description

It is generally recognised that the stress versus strain response of connective tissue has a characteristic J − shape, such that stiffening occurs at strains above about 30%, Purslow [33]. Additionally, the stress level increases with increasing strain rate. Since the response is strain rate dependent, a strain energy density function does not exist for the material. Despite this deficiency, rubber elasticity models provide a useful phenomenological description of the shape of the stress versus strain curve for a given value of strain rate. The Mooney-Rivlin model has frequently been used to model soft tissue [34]. However, Shergold et al. [12] show that the Ogden [35] model for an incompressible, isotropic, hyper-elastic solid describes a wide range of strain hardening characteristics for the dermis. The one-term Ogden strain energy density function is given as:

$$\phi = \frac{2\mu}{\alpha^2}\left(\lambda_1^\alpha + \lambda_2^\alpha + \lambda_3^\alpha - 3\right) \tag{1}$$

where ϕ is the strain energy density per undeformed unit volume, λ is the stretch ratio, α is the strain hardening exponent and μ is the shear modulus. The principal values of nominal stress σ_i $(i = 1, 2, 3)$ are related to the principle stretches λ_i by

$$\sigma_i = \frac{\mathrm{d}\phi}{\mathrm{d}\lambda_i} - p \tag{2}$$

where p is the hydrostatic pressure. Shergold et al. [12] argue that the characteristic J-curve is due to alignment of collagen fibres, the degree of fibre alignment is insensitive to strain rate, and hence the strain hardening exponent α is strain rate independent. In contrast, the shear modulus is expected to increase with strain rate as it is determined by the rate dependence of the collagen fibres and the surrounding matrix. It will be shown below that the one term Ogden model is adequate to describe the uniaxial compression data of porcine adipose tissue.

During uniaxial compression the specimen is assumed to be in a state of uniaxial stress with the z-axis of a Cartesian co-ordinate system aligned with the direction of the applied load. Therefore,

$$\sigma_x = \sigma_y = 0 \tag{3}$$

For an incompressible solid in which the volume is conserved the principal stretch ratios are related by

$$\lambda_x = \lambda_y = \frac{1}{\sqrt{\lambda_z}} \tag{4}$$

and λ_i is related to strain ε_i by

$$\varepsilon_i = -\ln\lambda_i \tag{5}$$

Therefore, Equation (2) can be re-written as

$$\sigma = \frac{2\mu}{\alpha}\left[e^{-\varepsilon(\alpha-1)} - e^{\varepsilon\left(1+\frac{\alpha}{2}\right)}\right] \tag{6}$$

where α is a strain hardening exponent and μ is the shear modulus under infinitesimal straining.

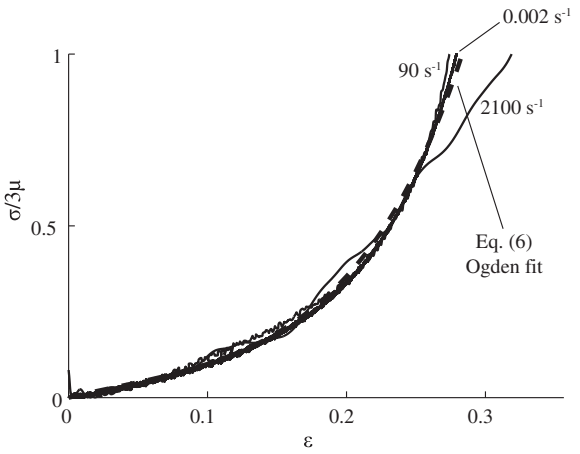

Fig. 10. A plot of normalised Ogden model, with $\alpha = 23$, compared to three representative stress versus strain curves for adipose tissue.

The Ogden model (1) has been fitted to the uniaxial compression data across the full range of strain rates tested. The shear modulus μ was taken as $E/3$ for each stress versus strain curve. A value of $\alpha = 23$ gives the best fit to the data, see Fig. 10. The average value of μ within each strain rate regime of testing is given in Table 1. Previous results for μ for the dermis are included and are taken from Shergold et al. [12]. For the dermis, the exponent α equals 12 over the full range of strain rates explored.

6. Concluding remarks

The constitutive properties of adipose tissue have been measured over a wide range of strain rate from 2×10^{-3} s^{-1}–5700 s^{-1}. The Young's modulus is almost insensitive to strain rate and has a value of 1 kPa, at strain rates below 10 s^{-1}. This value of modulus is three orders of magnitude less than that of the dermis. However, at higher strain rates, above 10 s^{-1}, the modulus of adipose tissue increases sharply while that of the dermis remains almost constant. Consequently, at a strain rate of 3000 s^{-1}, the modulus of adipose tissue is comparable to that of the dermis (about 4 MPa).

The shape of the compressive stress versus strain curve is similar across all strain rates, differing only by a scale factor which is conveniently given by the Young's modulus. This allows for a major simplification in description of the constitutive response. A one term Ogden strain energy density model can be used to adequately describe the data over the strain rates tested. This model comprises two parameters, the strain hardening exponent α (independent of strain rate) and the shear modulus μ (which scales with strain rate).

The authors find that adipose tissue behaves in an incompressible, non-linear manner and suggest that the Ogden multi-axial description is adequate at any given strain rate. Thus, the measured compressive response can be used to predict the multi-axial behaviour in a wide range of applications, such as those listed in the introduction to the paper. The fully reversed loading tests confirm that the shape of the stress-strain curve in tension is the same as that in compression. The issue of the failure of adipose tissue under a range of stress states and strain rates is left as a topic for future study.

Acknowledgements

The authors are grateful for financial support from the EPSRC, from Novo Nordisk A/S, Denmark and Cambridge University Multi-imaging centre for their support and assistance.

Appendix A. Development of a polymeric split Hopkinson pressure bar test rig

Split Hopkinson pressure bar (SHPB) tests using metallic pressure bars are insufficiently sensitive to measure the stress versus strain response of soft tissue. It is demonstrated here that polycarbonate (PC) pressure bars (with a Young's modulus of 3 GPa) are adequate for high strain rate tests on adipose tissue. First, a number of checks are made which confirm the elastic response of the PC bars. The purpose of Appendix A is to demonstrate that wave propagation in PC bars during SHPB tests is essentially elastic, and that viscoelastic effects are negligible. Analysis of the data can, therefore, be made using the theory of elastic wave propagation. To the authors' knowledge this has not been explicitly demonstrated before.

Design of a polycarbonate split Hopkinson pressure bar (SHPB)

A typical split Hopkinson pressure bar (SHPB) has input and output bars of uniform cross-sectional area A_b and modulus E_b. A specimen of length l and cross-sectional area A_h is placed between the bars. A derivation of the equations used to calculate the average stress $\sigma_s(t)$, strain $\varepsilon_s(t)$ and strain rate $\dot{\varepsilon}_s(t)$ within the specimen is given by Follansbee [36]. The measured strain level in the output bar is dependent upon the ratio of the stress in the specimen $\sigma_s(t)$ to the modulus of the bar E_b. If the specimen is very soft (as in the case of adipose tissue) the use of metallic pressure bars results in a low level of transmitted strain which may be difficult to distinguish from the inherent noise of the test equipment. Also, the input force cannot be measured precisely, which leads to difficulty in assessing whether force equilibrium exists within the specimen [37].

The strain sensitivity can be increased by substituting polymeric bars, which have substantially lower elastic moduli than metals. The improvement in sensitivity of the system enables lower stress levels to be measured, and permits a straightforward examination of force equilibrium in the specimen. This in turn gives confidence that the specimen is subjected to uniform deformation with negligible influence of internal wave reflections. In addition, as polymers exhibit lower wave speeds than metals, the specimen can be subjected to a longer test time, thereby enabling larger strains to be applied prior to the influence of waves reflected from the ends of the bars [36].

Polymeric bars typically exhibit viscoelastic rather than elastic behaviour which leads to a number of challenges for the analysis of the SHPB data. A series of validation exercises have been conducted to confirm that the PC pressure bars behave in an elastic rather than viscoelastic manner. A direct validation of the use of PC bars has also been achieved by comparing the high strain rate compression response of Divinycell HD250 PVC foam as measured by PC pressure bars and by magnesium alloy pressure bars.

Checks for elastic behaviour in polycarbonate bars

A series of checks are now reported which confirm that at low strain levels the PC bars behaved in an elastic manner.

The test set-up

A modified SHPB set-up comprising an input bar of length 2.2 m and a striker of length 0.25 m (Fig. A1) was used for the validation checks. Both bars were of diameter 12 mm. Pairs of resistance strain gauges were axially bonded near each end of the input bar, diametrically opposite to each other to check for bending. In order to avoid end effects the strain gauges were mounted 0.25 m from the end of the bars, which satisfies the established criterion of

mounting the gauges more than 10 bar diameters from the end of the bar [36]. The sensing circuitry and the calibration method were validated by performing a dummy test with no specimen present. Steel bars were employed, and the measured strain histories were found to be in good agreement with the predicted values (as given by elastic analysis).

Check 1: attenuation of wave in bar

The harmonic solution for the axial particle displacement $u(x,t)$ associated with the propagation of a longitudinal wave in a viscoelastic solid takes the form [38]

$$u = Ae^{\beta x}e^{i(\omega t+kx)} \tag{A1}$$

where β is the wave attenuation, ω is the angular frequency and k is the wave number. The minus sign corresponds to waves propagating in the positive x-direction. The level of attenuation is quantified by the parameter

$$\beta = \frac{\ln(\varepsilon_1/\varepsilon_2)}{x_g} \tag{A2}$$

where ε_1 and ε_2 are the maximum strains measured by the first and second strain gauges respectively, as shown in Fig. A1, and where $x_g = 1.7$ m is the distance between the strain gauges. A typical strain response at the two locations of the input bar is given in Fig. A2. The average measured level of attenuation was $\beta = 0.012$ m^{-1}. This level of attenuation is considered to be insignificant for selected values of striker velocities v in the range 4–13 ms^{-1}.

Check 2: measurement of dispersion

The strain gauge measurements revealed that the strain pulse progressing along the input PC bar is a well-defined square wave (see the typical example shown in Fig. A2). A small viscoelastic tail is present in the pulse measured at the second strain gauge. However, it is significantly smaller than the tails observed by Zhao et al. [37] for PMMA and is considered to be negligible. The wave-shape does not change significantly as the wave propagates along the bar. These are typical characteristics of an elastic bar.

High frequency oscillations are frequently evident in SHPB tests that employ metallic bars [21]. It is usual to design a 'pulse-shaper' made from a thin paper or copper disk, positioned between the striker bar and the input bar, to dampen out these unwanted oscillations [11]. However, the viscous properties of the PC bar are found to be sufficient to dampen the high frequency dispersion effects negating the need for a pulse-shaper.

Check 3: consistency check on the Young's modulus of PC

The Young's modulus of the bar can be predicted from the raw data in two ways [38]:

$$E = c_b^2\rho \tag{A3}$$

or

$$E = \frac{\rho v^2}{4\varepsilon_{\max}^2} \tag{A4}$$

where ρ is the density of the bar, c_b is the elastic wave speed, v is the velocity of the striker bar and $\varepsilon_{\max}$ is the peak height of the square strain pulse. The predictions according to the two methods are given in Table A1. They agree to within 5%, supporting the assertion that the PC bars can be treated as linear elastic.

Check 4: effect of strain amplitude upon the wave speed in the PC bar

The speed of an axial longitudinal elastic wave in a bar was measured explicitly from the time taken for the leading edge of the strain wave to travel between the strain gauges. Speed measurements were conducted for a range of peak strains in order to assess whether the wave speed is independent of strain level. The wave speed was not found to depend on strain for peak strains between 1000 με and 4500 με and had a mean value of 1495 ms^{-1}.

Check 5: Pochammer-Chree dispersion

Consideration of radial equilibrium for a compression wave propagating along a bar of finite diameter reveals dispersion effects, see Pochhammer [39] and Chree [40]. A representative input pulse has been assessed for dispersion using Bancroft's [41] solution to the Pochhammer–Chree equations. The level of dispersion was found to be negligible.

Check 6: Hopkinson bar tests on divinycell PVC HD250 foam

Validation of the test method was achieved by comparing the high strain rate response of a synthetic foam measured using PC pressure bars with the response recorded with metallic pressure bars. A high strain rate compression test was performed at a strain rate of 1500 s^{-1} on Divinycell PVC HD250 foam using PC bars; a repeat test was performed using AZM magnesium alloy pressure bars (supplied by Newmet Kock, Waltham Abbey) using the test set-up shown in Fig. 2. The observed responses overlap to within material scatter, see Fig. A3. The results are also in agreement with those obtained previously by Tagarielli et al. [42] using magnesium alloy pressure bars.

Fig. A1: Experimental set-up to investigate the propagation of strain waves in polycarbonate bars.

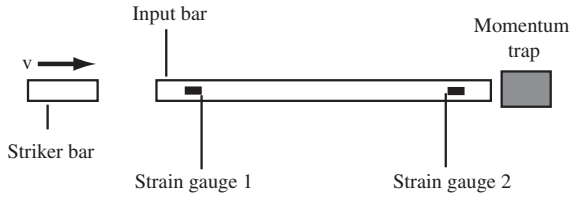

Fig. A2: Typical strain response of the long polycarbonate bar measured at two locations along the bar. The impact velocity of the striker is approximately $v = 10$ ms^{-1}. The distance between the first strain gauge and the second strain gauge is 1.7 m.

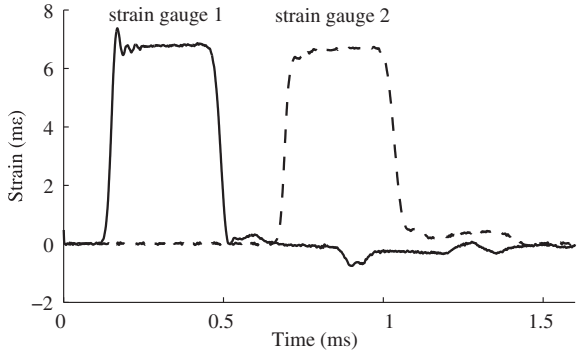

Fig. A3: Compression of Divinycell PVC HD250 foam. Results obtained with polycarbonate pressure bars are compared with results collected using magnesium pressure bars. The tests were conducted at a strain rate of 1500 s^{-1}.

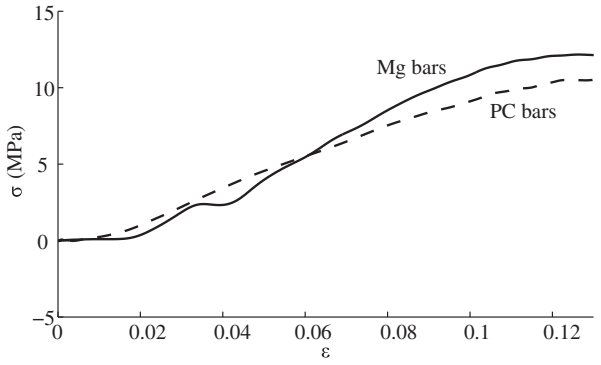

Table A1
Strain wave analysis of polycarbonate bars. ±1 standard deviation is also shown.

c_b (m/s)	β (1/m)	E (GPa) from Eq. (A3)	E (GPa) from Eq. (A4)
1495 ± 10.7	0.012 ± 16 × 10^{-4}	4.03 ± 0.057	3.84 ± 0.002

Appendix B. Application of the polycarbonate Hopkinson bar to adipose tissue

The results presented above establish that PC pressure bars behave in an elastic manner at the strain levels employed in SHPB tests. However, use of the SHPB to measure the high strain rate response of adipose tissue also requires a consideration of axial and radial equilibrium within the specimen.

A representative measure of the stress versus strain response (at $\dot{\varepsilon} = 3500\ s^{-1}$) is given in Fig. B1. It is observed that there is an initial transient in the axial stress with a peak value of 0.5 MPa over an initial compression phase of 10% strain. It is argued below that this transient is due to the radial acceleration of material elements (as the velocity of the front face rises from zero to the order of 10 m/s). This additional inertial stress is subtracted from the measurement in order to obtain the material stress versus strain response.

Radial inertial effects in the specimen

Samanta [43] has extended the work of Davies and Hunter [44] and Kolsky [13] to estimate the level of axial stress associated with the radial inertia of the specimen. The inertial contribution σ_I to the axial stress comprises a term σ_{vel} associated with the velocity v of the front face of the specimen, and a term σ_{accel} associated with the acceleration $\mathrm{d}v/\mathrm{d}t$ of the front face of the specimen, such that

$$\sigma_{\text{vel}} = \frac{3}{16}\rho\frac{d^2}{l^2}v^2 \tag{B1}$$

$$\sigma_{\text{accel}} = \rho\left(\frac{d^2}{8l}+\frac{l}{3}\right)\frac{\mathrm{d}v}{\mathrm{d}t} \tag{B2}$$

and

$$\sigma_I = \sigma_{\text{vel}} + \sigma_{\text{accel}} \tag{B3}$$

Here, d is the radius of the specimen, and l is the height of the specimen.

Now substitute for some typical values. Consider a test performed on a specimen of length $l = 2.3$ mm at $\dot{\varepsilon} = 3500\ s^{-1}$. The velocity of the front, impacted face of the specimen rises to a value of $v = 8\ ms^{-1}$ over the first 30 μs. Numerical differentiation of the velocity profile suggests that acceleration of the material reaches a peak value of $\mathrm{d}v/\mathrm{d}t = 3 \times 10^5\ ms^{-2}$. The contributions of σ_{vel} and σ_{accel} to the inertial stress σ_I, of a specimen tested at $\dot{\varepsilon} = 3500\ s^{-1}$ are shown in Fig. B1 and are compared to the measured stress versus strain curve. The peak value of σ_I is approximately 0.2 MPa at 2% strain and falls to zero by 5% strain. This analysis indicates that at strain levels below 5% the stress measurement is dominated by the inertial stress. All subsequent interpretation of the data at high strain rates is, therefore, restricted to measurements made at 8% strain and above. The Young's modulus is taken to be the secant value at a strain level of 10%, in order to disregard the axial and radial inertial contributions.

Check on axial equilibrium in the specimen

Davis and Hunter [44] have demonstrated that a specimen achieves axial equilibrium once an elastic stress wave has passed along its length approximately three times. The time taken for the stress wave to traverse the specimen length is given by l/c_s, where l is the length of the specimen and the elastic wave speed c_s depends upon the bulk modulus K according to $c_s=(K/\rho)^{1/2}$ [38]. The density ρ of adipose tissue is 920 kgm^{-3}. Saraf et al. [45] have estimated the bulk modulus of biological tissue to be 0.5 GPa, giving a wave speed of approximately 700 ms^{-1}. For a specimen length of 3 mm the time taken to reach axial equilibrium is just over 4 μs, corresponding to an initial strain of 0.8%. On this basis, axial equilibrium can be taken to hold from the outset of the test.

A further check on the state of equilibrium can be made by comparing the stress level on the face of the input bar ($\sigma_i + \sigma_r$) with the stress on the face of the output bar (σ_t). A comparison of the input and output stress from a test at a strain rate of 2000 s^{-1} is shown in Fig. B2. A slight mismatch in the identification of the start of the input and reflected pulse has resulted in errors in the measurement of the input stress. However, it is clear from this comparison that the axial equilibrium has been achieved within the first 40 μs of the test, which corresponds to an axial strain of about 8%. Again, this suggests that a secant value of Young's modulus at an axial strain of 10% is appropriate.

Fig. B1: Comparison of the measured stress with the inertial stresses σ_{vel} and σ_{accel}, described by Equations (B1) and (B2). The net response is the measured stress less the inertial stresses. The test was conducted at 3500 s^{-1}.

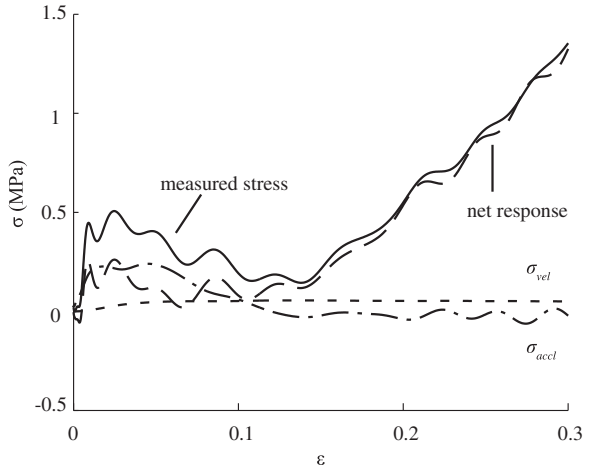

Fig. B2: Comparison of input ($\sigma_i + \sigma_r$) and output (σ_t) stress measured by the SHPB to assess the time to reach axial equilibrium. Measurements were taken at a nominal strain rate of 2000 s^{-1}.

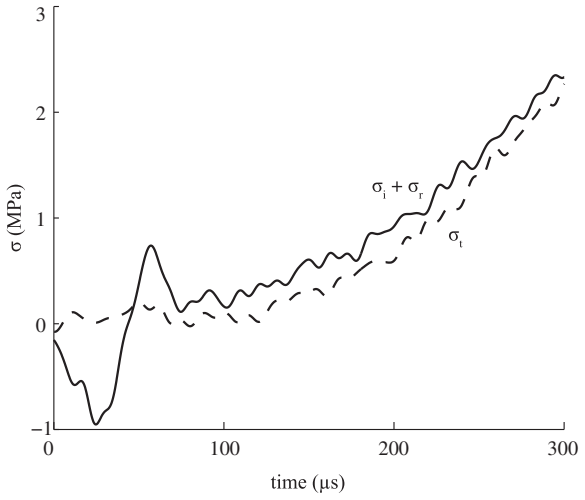

References

[1] Shergold OA, Fleck NA. Mechanisms of deep penetration of soft solids, with application to the injection and wounding of skin. Proceedings of the Royal Society of London: Series A 2004;460:3037–58.

[2] Comley KSC, Fleck NA. A micromechanical model of the modulus of adipose tissue. International Journal of Solids and Structures 2010;47:2982–90.

[3] Greenwood MRC, Johnson PR. The adipose tissue. In: Weiss L, editor. Histology, cell and tissue biology. Macmillan; 1983. p. 178–99.

[4] Samani A, Bishop J, Luginbuhl C, Plewes DB. Measuring the elastic modulus of ex vivo small tissue samples. Physics in Medicine and Biology 2003;48:2183–98.

[5] Hvidberg E. Water-binding by connective tissue and the acid mucopolysaccharides of the ground substance. Acta Pharmacologica et Toxicologica 1960; 17:267–76.

[6] Guyton AC, Scheel K, Murphree D. Interstitial fluid pressure. 3. Its effect on resistance to tissue fluid mobility. Circulation Research 1966;19:412–9.

[7] Miller-Young JE, Duncan NA, Baroud G. Material properties of the human calcaneal fat pad in compression: experiment and theory. Journal of Biomechanics 2002;35:1523–31.

[8] Zheng YP, Mak AFT. Extraction of quasi-linear viscoelastic parameters for lower limb soft tissues from manual indentation experiment. ASME Journal of Biomechanical Engineering 1999;121:330–9.

[9] Huang C-Y, Stankiewcz A, Ateshian GA, Mow VC. Anisotropy, inhomogeneity, and tension-compression nonlinearity of human glenohumeral cartilage in finite deformation. Journal of Biomechanics 2005;38:799–809.

[10] Mansour JM, Davis BR, Srour M, Theberge R. A method for obtaining repeatable measurements of the tensile properties of skin at low strain. Journal of Biomechanics 1993;26:211–6.

[11] Song B, Chen W, Ge Y, Weerasooriya T. Dynamic and quasi-static compressive response of porcine muscle. Journal of Biomechanics 2007;40:2999–3005.

[12] Shergold OA, Fleck NA, Radford D. The uniaxial stress versus strain response of pig skin and silicone rubber at low and high strain rates. International Journal of Impact Engineering 2006;32:1384–402.

[13] Kolsky H. An investigation of the mechanical properties of materials at very high rates of loading. Proceedings of the Royal Society of London, Series B 1949;62:676–700.

[14] Dioh NN, et al. Stress wave propagation effects in split Hopkinson pressure bar tests. Proceedings of the Royal Society of London, Series A 1995;449:187–204.

[15] Wang L, Labbibes K, Asari Z, Pluvinage G. Generalization of split Hopkinson bar technique to use viscolelastic bars. International Journal of Impact Engineering 1992;15:669–86.

[16] Aleyaasin M, Harrigan JJ. Wave dispersion and attenuation in viscoelastic polymeric bars: analysing the effect of lateral inertia. International Journal of Mechanical Sciences 2010;52:754–7.

[17] Zhao H, Gary G. A 3-Dimensional Analytical solution of the longitudinal-wave propagation in an Infinite linear viscoelastic cylindrical bar – application to experimental-Technique. Journal of the Mechanics and Physics of Solids 1995; 43:1335–48.

[18] Deshpande VS, Fleck NA. High strain rate compressive behaviour of aluminium alloy foams. International Journal of Impact Engineering 2000;24:277–98.

[19] Douglas WR. Pigs and Men and Research – review of applications and Analogies of pig, Sus Scrofa, in Human Medical-Research. Space Life Sciences 1972;3:226–34.

[20] Dally JW, Riley WF. Experimental stress analysis. 3rd ed. McGraw-Hill International Editions; 1991.

[21] Follansbee PS, Frantz C. Wave-propagation in the split Hopkinson pressure bar. Journal of Engineering Materials and Technology-Transactions of the ASME 1983;105:61–6.

[22] Doebelin EO. Measurement systems: application and design. McGraw-Hill; 1966.

[23] Fleck NA. Some aspects of clip gauge design. Strain 1983;19:17–22.

[24] Sawas O, Brar NS, Brockman RA. Dynamic characterisation of compliant materials using an all-polymeric split Hopkinson bar. Experimental Mechanics 1998;38:204–10.

[25] Van Houten EEW, Doyley MM, Kennedy fE, Weaver JB, Paulsen KD. Initial in vivo Experience with Steady-state Subzone-based MR Elastography of the human breast. J Mag Resonance Imaging; 2003.

[26] Elliott DM, Setton LA. Anisotropic and inhomogeneous tensile behavior of the human anulus fibrosus: experimental measurement and material model predictions. Journal of Biomechanical Engineering-Transactions of the ASME 2001;123:256–63.

[27] Bonfield W, Grynpas MD. Anisotropy of Young's modulus of bone. Nature 1977;270:453–4.

[28] Patel PN, Smith CK, Patrick CW. Rehological and recovery properties of poly(ethylene glycoll) diacrylate hydrogels and human adipose tissue. Journal of Biomedical Materials Research Part A 2005;73A:313–9.

[29] Geerligs M, Peters GWM, Ackermans PAJ, Oomens CWJ, Baaijens FPT. Linear viscoelastic behavior of subcutaneous adipose tissue. Biorheology 2008;45: 677–88.

[30] Nightingale K, McAleavey S, Trahey G. Shear-wave generation using acoustic radiation force: in vivo and ex vivo results. Ultrasound in Medicine and Biology 2003;29:1715–23.

[31] Gefen A, Haberman E. Viscoelastic properties of ovine adipose tissue covering the gluteus muscles. ASME Journal of Biomechanical Engineering 2007;129: 924–30.

[32] Van Sligtenhorst C, Cronin DS, Wayne Brodland G. High strain rate compressive properties of bovine muscle tissue determined using a split Hopkinson bar apparatus. Journal of Biomechanics 2006;39:1852–8.

[33] Purslow P. Notch-Sensitivity of Nonlinear materials. Journal of Material Science 1991;26:4468–76.

[34] Miller K, Chinzei K. Constitutive modelling of brain tissue experiment and theory. Journal of Biomechanics 1997;30:1115–21.

[35] Ogden RW. Large deformation isotropic elasticity – correlation of theory and experiment for incompressible Rubberlike solids. Proceedings of the Royal Society of London: Series A 1972;326:565–84.

[36] Follansbee PS. The Hopkinson bar. In: Kuhn EH, Medlin D, editors. ASM handbook: volume 8 mechancial testing and evaluation. ASM International; 1985. p. 198–217.

[37] Zhao H, Gary G, Kelpaczko JR. On the use of viscoelastic split Hopkinson pressure bar. International Journal of Impact Engineering 1997;19:319–30.

[38] Kolsky H. Stress waves in solids. Oxford University Press; 1953.

[39] Pochhammer L. The Journal of Pure and Applied Mathematics 1876;81: 324–36.

[40] Chree C. The equations of an isotropic elastic solid in polar and cylindrical co-ordinates. Transactions of the Cambridge Philosophical Society 1889;14: 251–369.

[41] Bancroft D. The velocity of longitudinal waves in cylindrical bars. Physics Review 1941;59:588–93.

[42] Tagarielli VL, Deshpande VS, Fleck NA. The high strain rate response of PVC foams and end-grain balsa wood. Composites Part B: Engineering Marine Composites and Sandwich Structures 2008;39:83–91.

[43] Samanta SK. Dynamic deformation of aluminium and copper at elevated temperatures. Journal of the Mechanics and Physics of Solids 1971;19: 117–22.

[44] Davies EDH, Hunter SC. The dynamic compression testing of solids by the method of the split Hopkinson pressure bar. Journal of the Mechanics and Physics of Solids 1963;11:155–79.

[45] Saraf H, Ramesh KT, Lennon AM, Merckle AC, Roberts JC. Mechanical properties of soft human tissues under dynamic loading. Journal of Biomechanics 2007;40:1960–7.